J|A|C|S
ARTICLES
Published on Web 02/24/2007

Growth and Characterization of Films Containing Fullerenes and Water Soluble Porphyrins for Solar Energy Conversion Applications

Vito Sgobba,[†] Gabriele Giancane,[‡] Sabrina Conoci,[§] Serena Casilli,[‡] Giampaolo Ricciardi,[||] Dirk M. Guldi,[†] Maurizio Prato,[⊥] and Ludovico Valli*[,‡]

Contribution from The Institute for Physical Chemistry, Friedrich-Alexander-Universität, Erlangen-Nürnberg, 91058 Erlangen, Germany, the Dipartimento di Ingegneria dell'Innovazione, Università degli Studi di Lecce, Via Prov.le Lecce-Monteroni, 73100 Lecce, Italy, LabonChip R&D, Microfluidic Division CPG, STMicroelectronics, Stradale Primosole, 50, I-95121 Catania, Italy, the Dipartimento di Chimica, Università della Basilicata, Via N. Sauro, 85, 85100 Potenza, Italy, and the Dipartimento di Scienze Farmaceutiche, Università degli Studi di Trieste, Piazzale Europa, 1, 34127 Trieste, Italy

Received August 2, 2006; E-mail: ludovico.valli@unile.it

Abstract: Thin films consisting of two fulleropyrrolidine derivatives **1** or **2** and a water-soluble porphyrin, **TPPS$_4$**, were prepared by the Langmuir−Schäfer (LS, horizontal lifting) method. In particular, a solution of the fulleropyrrolidine in chloroform and dimethyl sulfoxide was spread on the water surface, while the porphyrin (bearing peripheral anionic sulfonic groups) was dissolved into the aqueous subphase. To the best of our knowledge, such a versatile method for film fabrication of fullerene/porphyrin mixed composite films has never been used by other researchers. Evidence of the effective interactions between the two components at the air−water interface was obtained from the analysis of the floating layers by means of surface pressure vs area per molecule Langmuir curves, Brewster angle microscopy, and UV−visible reflection spectroscopy. The characterization of the LS films by UV−visible spectroscopy reveals that in each case the two constituents behave as strongly interacting π systems. The use of polarized light suggests the existence of a preferential direction of the **TPPS$_4$** macrocyclic rings with an edge-on arrangement with respect to the substrate surface, regardless which fulleropyrrolidine derivative is in the composite film. Atomic force microscopy investigations give evidence of morphologically flat layers even for LS transfer at low surface pressures. Photoaction spectra were recorded from films deposited by only one horizontal lifting onto indium−tin−oxide (ITO) electrodes, and the observed photocurrent increased notably with increasing transfer surface pressure for both **1**/**TPPS$_4$** and **2**/**TPPS$_4$** composite films. IPCE values are larger for **2**/**TPPS$_4$** systems in comparison with **1**/**TPPS$_4$** composite layers. Finally, a nonconventional approach to photoinduced phenomena is proposed by differential spectroscopy in the FT−IR attenuated total reflectance (ATR) mode.

Introduction

Functional photovoltaic devices have been the focus of intense studies in the chemistry and physics of fullerenes.[1−3] Quite a number of fullerene derivatives have been synthesized and investigated to understand crucial phenomena such as energy transport and charge separation.[4−6] In fact, fullerene derivatives exhibit remarkable electron accepting properties,[7] which, together with the small reorganization energy,[8] make these compounds ideal components in photovoltaic devices.

Porphyrins and phthalocyanines have been very often used, as electron donors, in combination with fullerene derivatives,[9−14] though other donors have also given promising results.[15−19]

To structurally organize the donor and the acceptor units in efficient ways, lipid bilayer membranes,[20] electrostatic interactions,[21] LB films,[5] layer-by-layer depositions,[22] and self-assembled monolayers[23] have been devised. In this context, the LB technique represents one of the most flexible methods for

[†] Friedrich-Alexander-Universität.
[‡] Università degli Studi di Lecce.
[§] STMicroelectronics.
[||] Università della Basilicata.
[⊥] Università degli Studi di Trieste.

(1) Nierengarten, J.-F. *New J. Chem.* **2004**, *28*, 1177.
(2) Prato, M. *J. Mater. Chem.* **1997**, *7*, 1097.
(3) Prato, M. *Top.Curr. Chem.* **1999**, *199*, 173.
(4) Thomas, K. G. *Electrochem. Soc. Interf.* **1999**, *8*, 30.
(5) Tkachenko, N. V.; Vehmanen, V.; Nikkanen, J.-P.; Yamada, H.; Imahori, H.; Fukuzumi, S.; Lemmetyinen, H. *Chem. Phys. Lett.* **2002**, *366*, 245.
(6) van Hutten, P. F.; Hadziioannou, *G. Monatsh. Chem.* **2001**, *132*, 129.
(7) Allemand, P. M.; Koch, A.; Wudl, F.; Rubin, Y.; Diederich, F.; Alvarez, M. M.; Anz, S. J.; Whetten, R. L. *J. Am. Chem. Soc.* **1991**, *131*, 1050.
(8) Guldi, D. M. In *The small reorganization energy of fullerenes in Fullerenes: From Synthesis to Optoelectronic Properties*; Guldi, D. M., Martin, N., Eds.; Kluwer Academic Publishers: 2002; Chapter 8, pp 237−265.
(9) Sariciftci, N. S.; Wudl, F.; Heeger, A. J.; Maggini, M.; Scorrano, G.; Prato, M.; Bourassa, J.; Ford, P. C. *Chem. Phys.* **1995**, *247*, 510.
(10) Imahori, H.; Hagivara, K.; Aoki, M.; Akiyma, T.; Tanigushi, S.; Okada, T.; Shirakava, M.; Sakata, Y. *J. Am. Chem. Soc.* **1996**, *118*, 11771.

 10.1021/ja0655789 CCC: $37.00

Chart 1. Structure of Fullerene Derivatives **1** and **2** and of 5,10,15,20-Tetraphenyl-21*H*,23*H*-porphine Tetrasulfonate (**$TPPS_4$**)

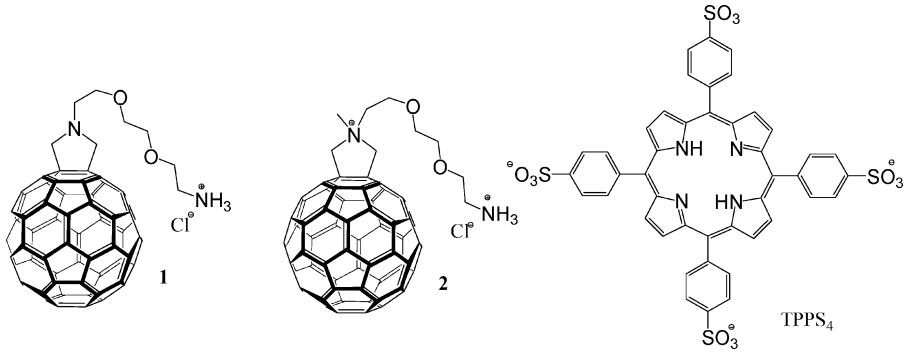

the preparation of homogeneous multilayers, guaranteeing control over molecular organization, film thickness, composition, and architecture.[24]

Uniform Langmuir films of C_{60} and C_{60}-derivatives on the water surface are difficult to obtain, because of the tendency of fullerenes to generate 3D intermolecular $\pi-\pi$ aggregates.[25] Among the many parameters that have been shown to impact the floating film properties the concentration of the spreading solutions (dilute solutions give better results), the volume of the starting solution spread at the air−water interface and pH and composition of the subphase should be considered with care.[26] Several parameters to achieve the formation of true and stable monolayers of C_{60} derivatives have been identified: (a) preparation of fullerene derivatives bearing strongly polar hydrophilic head groups; (b) achievement of a reasonable balance between the hydrophobic and hydrophilic portions of the molecule; (c) an adequate distance between the hydrophilic head group and the C_{60} sphere in order to allow better interaction with the water subphase; (d) preferential introduction of aliphatic chains sustaining a polar group with large sterical hindrance to minimize the attractive $\pi-\pi$ interactions.[26]

In the present work, we use coulomb interactions between cationic fullerene derivatives at the water surface and anionic porphyrins dissolved in the water subphase to deposit monolayer dyad films. The structures of used fullerene and porphyrin derivatives are illustrated in Chart 1. The resulting films were transferred via the Langmuir−Schäfer method, that is, horizontal lifting of the electrostatically induced donor−acceptor systems.[27] In particular, our efforts focused on improving the performances of charge-separated radical ion pair states for photovoltaic purposes, through the systematic variation of C_{60} derivatives (i.e., charge and/or modulation of surface pressure in the construction of different films). The intimate contiguity of the two components can trigger the exciplex generation, thus leading to efficient charge-transfer events.[13,28]

Results and Discussion

The value of the limiting area per molecule was obtained by extrapolating the steep ascending portion of the Langmuir curve to surface pressure $\Pi = 0$ mN/m. Importantly, for fullerene derivative **1** the limiting area per molecule is significantly lower than the value expected for a true monolayer of C_{60}. We estimate, for example, a value of 66 Å^2/molecule instead of the theoretical value 86.6 Å^2/molecule. The latter is based on the cross-sectional area of C_{60} and/or the intersphere distance in C_{60} crystals that show a dense hexagonal packing.[29−31] Implicit here is the existence of attractive $\pi-\pi$ interactions that result in extraordinarily stable 3D van der Waals aggregates. The cohesive energy in such aggregates is larger than 30 kcal mol^{-1}. From this we infer that the floating films are ill-defined with 3D fullerene domains more than an individual monolayer in thickness. The presence of a singly charged $-NH_3^+$ hydrophilic group is apparently insufficient to balance the hydrophobic character of the fullerene and to generate a real monolayer on the pure water surface. For **1**, more details on (i) Langmuir Π vs A curves, (ii) BAM images, and (iii) reflection spectroscopy, all at the air−water interface, are gathered in previous work.[32]

Next let us turn to the behavior when a water-soluble porphyrin is present in the aqueous subphase. Figure 1 documents the Langmuir curves of **1** in the absence and presence of **$TPPS_4$**. At first glance the two curves appear considerably different. The limiting areas for subphases of pure water or of

(11) Imahori, H.; Ozava, S.; Ushida, K.; Takahashi, S.; Azuma, T.; Ajavakom, A.; Akiyama, T.; Hasegawa, M.; Taniguchi, S.; Okada, T.; Sakata, Y. *Bull. Chem. Soc. Jpn.* **1999**, *72*, 485.
(12) Helaja, J.; Tauber, A. Y.; Abel, Y.; Tkachenko, N. V.; Lemmetyinen, H.; Kilpeläinen, I.; Hynninen, P. H. *J. Chem. Soc., Perkin Trans. 1* **1999**, 2403.
(13) Tkachenko, N. V.; Rantala, L.; Tauber, A. Y.; Helaja, J.; Hynninen, P. H.; Lemmetyinen, H. *J. Am. Chem. Soc.* **1999**, *121*, 9378.
(14) Alekseev, A. S.; Tkachenko, N. V.; Tauber, A. Y.; Hynninen, P. H.; Osterbacka, R.; Stubb, H.; Lemmetyinen, H. *Chem. Phys.* **2002**, *275*, 243.
(15) Kuciauskas, D.; Lin, S.; Seely, G. R.; Moore, A. L.; Moore, T. A.; Gust, D. *J. Phys. Chem.* **1996**, *100*, 15926.
(16) Guldi, D. M.; Maggini, M.; Scorrano, G.; Prato, M. *J. Am. Chem. Soc.* **1997**, *119*, 974
(17) Imahori, H.; Sakata, Y. *Adv. Mater.* **1997**, *9*, 537
(18) Naito, K.; Sakurai, M.; Egusa, S. *J. Phys. Chem. A* **1997**, *101*, 2350
(19) Martin, N.; Sanchez, L.; Illescas, B.; Perez, I. *Chem. Rev.* **1998**, *98*, 2527.
(20) Sakata, Y.; Tatemitsu, H.; Bienvenue, E.; Seta, P. *Chem. Lett.* **1988**, 1625.
(21) Jiang, H.; Su, W.; Hazel, J.; Grant, J.T.; Tsukruk, V. V.; Cooper, T. M.; Bunning, T. J. *Thin Solid Films* **2000**, *372*, 85.
(22) Guldi, D. M.; Pellarini, F.; Prato, M.; Granito, C.; Troisi, L. *Nano Lett.* **2002**, *2*, 965.
(23) Arias, F.; Godínez, L. A.; Wilson, S. R.; Kaifer, A. E.; Echegoyen, L. *J. Am. Chem. Soc.* **1996**, *118*, 6086
(24) Petty, M. C. *Langmuir-Blodgett films: an introduction*; Cambridge University Press: Cambridge, 1996.
(25) Gao, Y.; Tang, Z.; Watkins, E.; Majewski, J.; Wang, H.-L. *Langmuir* **2005**, *21*, 1416.
(26) Leo, L.; Mele, G.; Rosso, G.; Valli, L.; Vasapollo, G.; Guldi, D. M.; Mascolo, G. *Langmuir* **2000**, *6*, 4599.
(27) Honciuc, A.; Jaiswal, A.; Gong, A.; Ashworth, K.; Spangler, C. W.; Peterson, I. R.; Dalton, L. R.; Metzger, R. M. *J. Phys. Chem. B* **2005**, *109*, 857.
(28) Imahori, H.; Ozava, S.; Ushida, K.; Takahashi, S.; Azuma, T.; Ajavakom, A.; Akiyama, T.; Hasegawa, M.; Taniguchi, S.; Okada, T.; Sakata, Y. *Bull. Chem. Soc. Jpn.* **1999**, *72*, 485
(29) Krätschmer, W.; Lamb, L. D.; Fostiropoulos, K.; Huffman, D. R. *Nature* **1990**, *347*, 354.
(30) Stephens, P.W.; Mihaly, L.; Lee, P. L.; Whetten, R. L.; Huang, S. M.; Kaner, R.; Diederich, F.; Holczer, K. *Nature* **1991**, *351*, 632.
(31) Heiney, P. A.; Fisher, J. E.; McGhie, A. R.; Romanow, W. J.; Denenstein, A. M.; McCauley, J.P., Jr.; Smith, A. B., III; Cox, D. E. *Phys. Rev. Lett.* **1991**, *66*, 2911.
(32) Conoci, S.; Guldi, D.; Nardis, S.; Paolesse, R.; Kordatos, K.; Prato, M.; Ricciardi, G.; Vicente, M. G. H.; Zilbermann, I.; Valli, L. *Chem.−Eur. J.* **2004**, *10*, 6523.

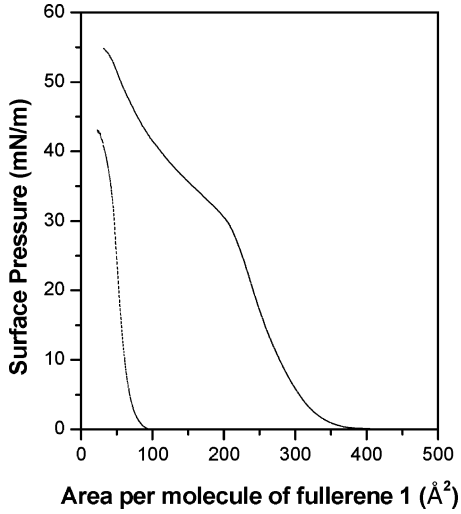

Figure 1. Surface pressure Π vs area per molecule of fullerene derivative **1** curves for pure water as subphase (dotted line) and when the subphase contains **TPPS$_4$** (continuous line).

a porphyrin solution are 66 and 302 Å^2 per **1**, respectively. Such a marked difference suggests effective interactions between **1** and **TPPS$_4$**. Reflection spectroscopy will further substantiate the increased surface area. It is, nevertheless, safe to conclude that the four anionic $-SO_3^-$ groups of **TPPS$_4$** promote, through efficient electrostatic interactions with $-NH_3^+$ of **1**, the generation of a homogeneous floating layer.

Brewster angle microscopy (BAM) has been remarkably effective when investigating floating films (i.e., on a scale of 1 μm) at the air−water interface: it is particularly suited for the identification of phase transitions, segregations, and film collapses.[33] BAM is a noninvasive technique, since it does not necessitate the introduction of, for example, fluorescent probes during the visualization of floating cluster reorganization. Notable is also that, during the compression and the BAM investigation, reflection spectra (ΔR) were contemporaneously registered at different surface pressures.

Immediately after solvent evaporation (0 mN/m), heterogeneously shaped, disorganized 3D aggregates are discernible in the BAM images. Upon compression, a systematic enlargement of these 3D aggregates arise with, however, no apparent variation in the domain brightness. Implicit are mixed **1**/**TPPS$_4$** films, whose formation is governed by uneven packing. The absence of appreciable phase transitions is important, since it is consistent with the Π vs A pattern of the Langmuir curve. Figure 2 exemplifies the evolution of the floating layer morphology, in the range from 0 to 20 mN/m. In some cases large islands exhibited birefringence, which are indicative of regions with molecular alignment or organization.

The introduction of **TPPS$_4$** in the water subphase has a remarkable effect: avoidance of the generation of independent domains in mixed films of C_{60} and macrocycle derivatives, usually observed when blends of two such constituents are spread at the air−water interface. In fact, **TPPS$_4$** molecules probably intercalate among the C_{60} spheres thus producing clusters of intimately interacting donor−acceptor moieties. Increasing surface pressure, these clusters tend to coalesce giving rise to much larger domains.

(33) Hönig, D.; Möbius, D. *J. Phys. Chem.* **1991**, *95*, 4590.

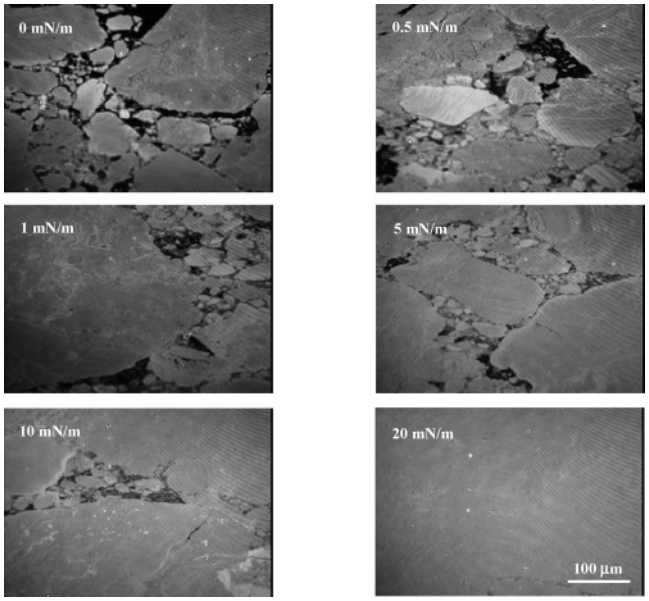

Figure 2. BAM images of **1**/**TPPS$_4$** obtained at different surface pressures (0, 0.5, 1, 5, 10, 20 mN/m).

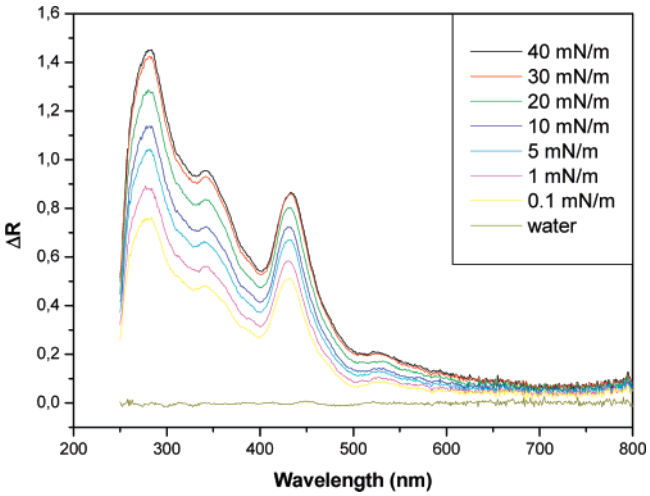

Figure 3. UV/vis reflection spectra of the **1**/**TPPS$_4$** mixture at the air−water interface and at different surface pressure values (T = 20 °C).

Next, interfacial phenomena were tested by reflection spectroscopy under normal incidence in the UV−visible range. In particular, the difference in reflectivity (ΔR) from the chromophore layer floating on the subphase and from the bare subphase surface was determined as a function of wavelength. These measurements were carried out directly with the floating films on the water surface.[34] Illustrative examples are shown in Figure 3, where reflection spectra are gathered of **1** on a **TPPS$_4$** containing subphase after reaching equilibrium at various surface pressures.

As Figure 3 illustrates, the most important characteristic is a new peak around 430 nm, which corresponds to the Soret band of **TPPS$_4$**. Notably, films of **1** that float on a pure water subphase lack this feature.[32] It is remarkable that the Soret is already apparent at surface pressures as low as 0.1 mN/m. This implies that **1**/**TPPS$_4$** interactions are activated as soon as the

(34) H. Kuhn, D. Möbius, *Monolayer assemblies, in Physical Methods of Chemistry, Vol. IXB, Investigations of Surfaces and Interfaces − Part B*; Rossiter, B.W.; Baetzold, R. C. Eds.; Wiley-Interscience: New York, 1993; pp 375−542.

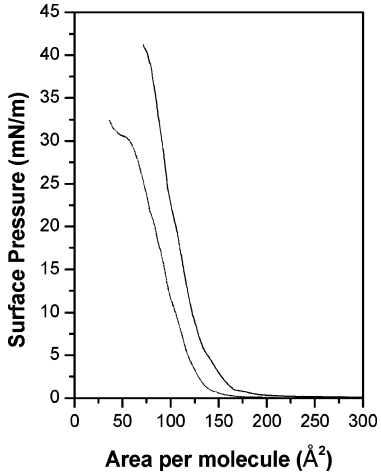

Figure 4. Langmuir curves of fullerene derivative **2** in the case of the pure water subphase (dotted line) and the subphase containing the water-soluble porphyrin (continuous line).

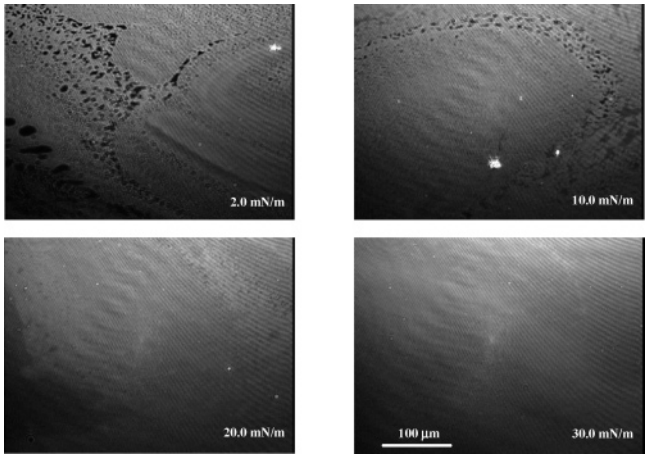

Figure 5. Brewster angle microscopy (BAM) images of **2** floating layers obtained at different surface pressure values (2, 10, 20, 30 mN/m). Stripes are interferences from the laser light.

solvent evaporation comes to an end: only those chromophores that are located at the air−water interface affect the enhanced reflection.[35] Accumulation of the tetraanionic **TPPS$_4$** at the interface via electrostatic interactions with the monocationic **1** is also substantiated by these spectra.

When compressing the films the surface density grows and the reflection enhances, while the overall pattern remains unaffected. The ΔR increase suggests that, after the initial aggregation, the self-organized and associated clusters are dragged onto the water surface and coalesce. In turn, the surface density of the floating layer is enhanced. It is worth noting that the reflection spectra undergo smaller and smaller variations during the compression processes. A possible rationale implies that the aggregated 3D domains are constrained together, but the floating film is too rigid to allow any reorganization. The spectral behavior is also consistent with the pattern seen in the Langmuir isotherm and with the information deduced from the BAM investigations.

The same electrostatic approach was probe interactions between **2** (i.e., bearing two positive charges) and **TPPS$_4$** at the air−water interface. Also in this case the characterizations were carried out by Langmuir Π vs A isotherms, BAM images, and reflection spectroscopy analysis. Figure 4 illustrates the Langmuir isotherms recorded for **2** on a pure water subphase (dotted line) and a subphase containing **TPPS$_4$** (solid line).

As in the case for **1**, the two curves for **2** differ remarkably. Thus, we postulate that even for **2** effective interactions must exist with **TPPS$_4$** that is dissolved in the aqueous subphase. The presence of **TPPS$_4$** causes a shift toward larger areas per molecule from 124 to 141 Å^2 per fullerene molecule.

Let us first look at **2**: A value of 124 Å^2 points out that an adequate balance between hydrophobic and hydrophilic parts ensures the formation of stable, pure Langmuir monolayers at the air−water interface. The presence of a liquid condensed phase in the floating films might be conjectured by the continuous onset of the surface pressure. Still, the BAM images reveal that **2** already associates at large areas. Moreover, the stability of such monolayers on the water surface is generally associated with a steep condensed phase branch of the curve, a high collapse pressure, and negligible hysteresis effects in compression−expansion cycles. In **2**, the two polar head groups are responsible for attractive interactions with the water subphase, inducing a two-dimensional arrangement at the air−water interface.

The above conclusions were further corroborated by BAM investigations. BAM images manifest homogeneous distributions of light intensities and hence a uniform, monomolecular Langmuir film. In fact, for all surface pressures that correspond to the condensed phase in the Langmuir curve (i.e., 12 mN/m $< \Pi <$ 30 mN/m) only homogeneous morphologies were registered. At molecular areas larger than 120 Å^2, BAM images indicate the presence of differently shaped black voids. These, which correspond to the pure water surface, evanesce when the surface pressure approaches 12 mN/m. Figure 5 reports the BAM images obtained at different surface pressures.

Electrostatic interactions between **2** and **TPPS$_4$** promote a film morphology that is considerably different from that seen for **2** alone. After solvent evaporation, we find, for instance, a layer that contains a large number of differently shaped and sized voids. When compressing that layer, the black regions of bare water surface are reduced and the generation of large fluctuating domains is seen. BAM images taken at different surface pressures (see Figure 6) clearly document such an evolution. The **2**/**TPPS$_4$** formation at the air−water interface has obvious effects also on the Langmuir isotherm: an expansion of the branch corresponding to the condensed phase has been observed together with a higher collapse pressure. This leads us to conclude that the floating layers are of improved stability.

As far as the reflection spectroscopy analysis of **2**/**TPPS$_4$** is concerned, the same considerations are valid that have already been described for **1**/**TPPS$_4$**. The Soret band of **TPPS$_4$** is again seen in the spectra registered at different surface pressures (see Figure 7).

Therefore, also for **2** and **TPPS$_4$** spectroscopic evidence points to interfacial phenomena. Interestingly, when comparing the Soret band of **TPPS$_4$** in a chloroform solution with that in the ΔR spectrum of the floating film on the water surface, a significant broadening is noted for the latter case; this is symptomatic for large 3D aggregates.[32]

(35) Ravaine, S.; Le Pecq, F.; Mingotaud, C.; Delhaes, P.; Hummelen, J. C.; Wudl, F.; Patterson, L. K. *J. Phys. Chem.* **1995**, 99, 9551.

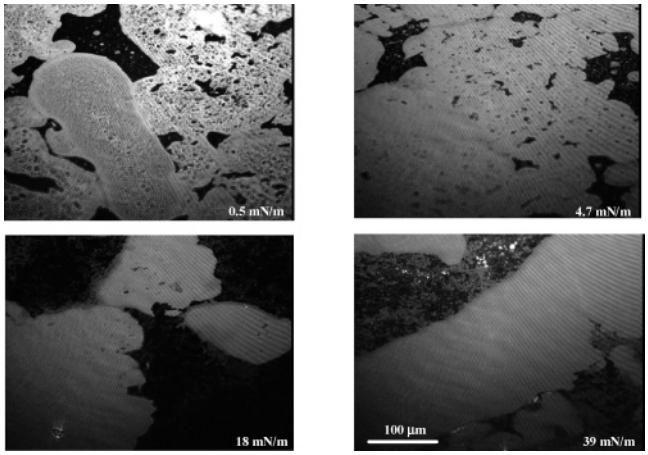

Figure 6. Brewster angle microscopy (BAM) images of the system **2**/**TPPS$_4$** obtained at different surface pressure values (0.5, 4.7, 18, 39 mN/m). Stripes are interferences from the laser light.

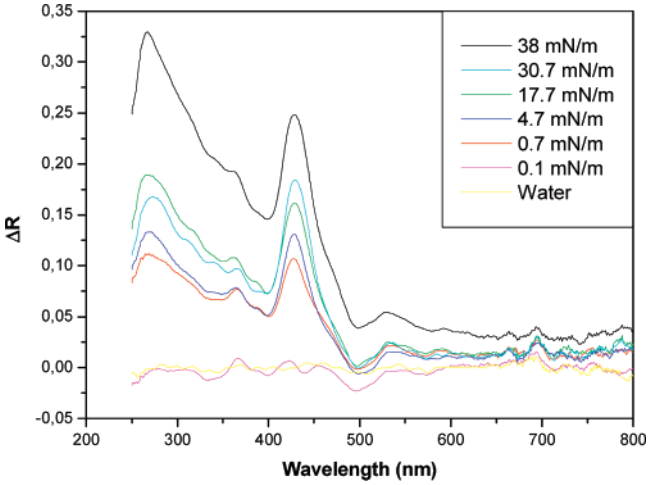

Figure 7. UV/vis reflection spectroscopy of the **2**/**TPPS$_4$** mixture on the water surface (T = 20 °C) at different surface pressures.

The photoactive films were first fabricated by the usual vertical Langmuir−Blodgett (LB) transfer. However, in these cases the films obtained were invariably of very poor quality with very low transfer ratios. Instead, the Langmuir−Schäfer (LS, horizontal lifting) method was successful; in fact, it is well-known for the deposition of rigid films which are typical at the two-dimensional solid region in the Langmuir curve, and the floating layers are also subject to less disruptive forces than those by the LB method.[24]

Ground state electronic absorption spectra of **1**/**TPPS$_4$** and **2**/**TPPS$_4$** for 30 layers and 40 layers, respectively, were recorded in the 200−1500 nm spectral range. Exemplifying, the 200 to 800 nm regions are compared in Figure 8.

Both spectra are dominated by the intense $\pi-\pi^*$ absorption features of **1** or **2** and **TPPS$_4$**, viz., a quite intense Soret band and four weak Q-bands. Additionally, a rather weak tail extends up to 1500 nm due to overlapping C−H and O−H bending vibrations,[32] fullerene electronic absorptions,[36] and tied interactions.

When correlating the fullerene $\pi-\pi^*$ absorption maxima with those of the porphyrin, notably higher ratios evolve for **1**/**TPPS$_4$**

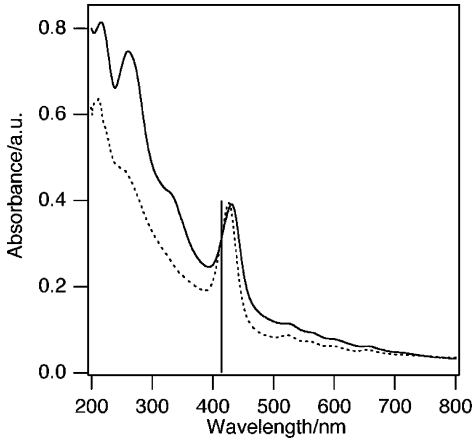

Figure 8. UV−visible absorption spectra of **1**/**TPPS$_4$** (30 layers) (full line) and **2**/**TPPS$_4$** (40 layers) (dashed line) thin films. The vertical line indicates the position of the Soret band maximum of **TPPS$_4$** in water solution.

multilayers than for **2**/**TPPS$_4$** multilayers. This prompts us to a higher fullerene/porphyrin stoichiometric ratio in the former case. A structural consideration helps to rationalize this observation: in **1** and **2** one and two cationic pyrrolidinium head groups are present, respectively, which per se limits in the **1**/**TPPS$_4$** multilayer a fullerene-to-porphyrin stoichiometric ratio of 4, while in **2**/**TPPS$_4$** the fullerene-to-porphyrin stoichiometric ratio might range between 2 and 4.

Despite the aforementioned differences, the spectra fail to be a linear combination of the individual components (i.e., **TPPS$_4$** and **1** or **2**). Instead, evidence for strong interactions between the two moieties constituting each multilayer is gathered. Relative to just **TPPS$_4$** in water, the Soret bands, as well as the Q bands, are broadened and shifted to longer wavelengths in **1**/**TPPS$_4$** and **2**/**TPPS$_4$** by about 18 and 13 nm, respectively. In the "quasi solid state" there is a considerable interaction between the $\pi-\pi^*$ systems of the two chromophores. We note that a progressive bathochromic shift of the Soret band has been observed upon spectroscopic titration of a face-to-face cyclic dimer of a zinc porphyrin with C_{60} in benzene.[37] Similarly, appreciable changes in the energy of the fullerene $\pi-\pi^*$ absorption maxima are seen. For example, the transitions in the 210−250 nm range are subject to a 8 nm blue-shift, when comparing the **2**/**TPPS$_4$** multilayer with that the corresponding fullerene reference in water.

Anion/cation interactions, due to different anion-to-cation ratios, are a likely explanation for the red-shifts of the **TPPS$_4$** spectral features in multilayers **of 1**/**TPPS$_4$** and **2**/**TPPS$_4$**. Indeed, interactions between the negatively charged sulfonatophenyl groups and the cationically charged fullerenes are expected to have a sizable impact on the energy of those **TPPS$_4$** MOs that are involved in the transitions underlying the B- and Q-bands. In this respect, the Gouterman-a_{2u}-derived MO is relevant, as it has large amplitudes on the meso-carbon atoms. Nonuniform destabilization of the a_{2u} orbitals is likely to contribute to the different red-shifts of these bands in the investigated multilayers. Charge-transfer effects and related subtle structural changes in the **TPPS$_4$** microenvironment, ultimately electronic effects, may also contribute to the generally low intensity of the **2**/**TPPS$_4$** spectrum relative to **1**/**TPPS$_4$**. In this context, the hypso-

(36) Li, J.; Zhang, S.; Zhang, P.; Liu, D.; Guo; Z.-X.; Ye, C.; Zhu, D. *Chem. Mater.* **2003**, 15, 4739.

(37) Tashiro, K.; Aida, T.; Zheng, J.-Y.; Kinbara, K.; Saigo, K.; Sakamoto, S.; Yamaguchi, K. *J. Am. Chem. Soc.* **1999**, *121*, 9477.

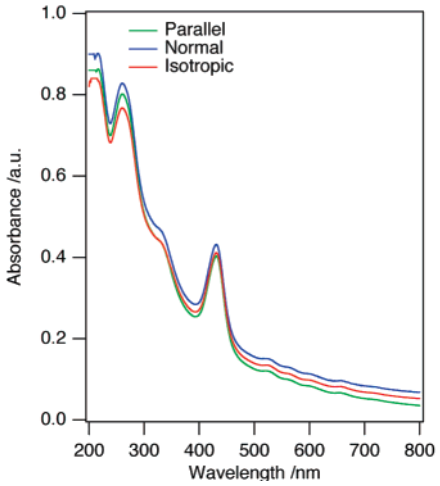

Figure 9. Electronic absorption spectra in isotropic light (red line) and polarized light of the **1**/**TPPS$_4$** Langmuir−Schäfer film (30 layers): electric field vector parallel to the incidence plane (green line); electric field vector normal to the incidence plane (blue line).

chromism seen in the porphyrin spectral features when strongly interacting with fullerenes should be considered.[37]

Next **1**/**TPPS$_4$** and **2**/**TPPS$_4$** films were investigated with polarized light (i.e., parallel or perpendicular to the incidence plane of radiation at an incidence angle $I = 0°$). All transitions (i.e., **1**, **2** and **TPPS$_4$**) show a small but notable dependence on the direction of the electric field vector. Figure 9, where **1**/**TPPS$_4$** is reported, implies, for example, that a non-negligible molecular order is present within the thin film. Safe predictions on the ordering of the fullerene subunits can hardly be made on the basis of these observed spectral changes. However, analysis of the dichroic ratios measured for the porphyrin absorptions prompts us to a trend, where the **TPPS$_4$** rings are preferentially edge-on oriented with respect to the quartz surface, regardless of the changes in the chemical composition of the investigated multilayers.

Atomic force microscopy (AFM) inspection of the monolayers of both **1**/**TPPS$_4$** and **2**/**TPPS$_4$** deposited onto hydrophobic silicon substrates at deposition pressure of 2, 5, 10, 20, and 25 mN/m, respectively, are reported in Figures 10 and 11.

Morphologically flat layers of **1**/**TPPS$_4$** and **2**/**TPPS$_4$** that cover homogenously the substrate surface are already discernible at low deposition pressures. Some differences are, however, evident when the monolayers of **1**/**TPPS$_4$** and **2**/**TPPS$_4$** are compared. At the lowest deposition pressure of 2 mN/m, the **1**/**TPPS$_4$** layer is not uniformly distributed over the substrate surface. In particular, the film features irregular vertical morphology with a 30% height variation: the range is between 2.0 and 3.0 nm; see Figures 10a and 11a. The measured root-mean-square roughness (rms) of this sample is ca. 1.9 nm. On the contrary, **2**/**TPPS$_4$** layers, at the same deposition pressure, have the general appearance of homogeneously dispersed and interconnected circles that are hundreds of nanometer (700−1800 nm) in diameter and 5.2 nm in height. Thus the **2**/**TPPS$_4$** layer is significantly higher than the **1**/**TPPS$_4$** layer (i.e., 5.2 nm vs 2−3 nm) but more uniform in vertical distribution. For such a reason the measured rms of the system **2**/**TPPS$_4$** is lower than that in the case of **1**/**TPPS$_4$** (1.0 nm vs 1.9 nm).

By increasing the deposition pressure from 5 to 25 mN/m, both systems give rise to uniformly and densely packed monolayers. In particular, a monolayer of **1**/**TPPS$_4$** (Figure 10b−d) at 5 mN/m covers uniformly and almost completely the substrate surface (Figure 10b). The measured rms is ca. 0.4 nm. Please note that the hydrophobic silicon substrate shows rms values of about 0.2 nm. At higher pressures (i.e., 10, 20 and 25 mN/m) the surface covering is more uniform with rms values of 0.4, 0.4, and 0.7, respectively (Figure 10c−e). Microcracks are featured for **2**/**TPPS$_4$** at a pressure of 5 mN/m. These

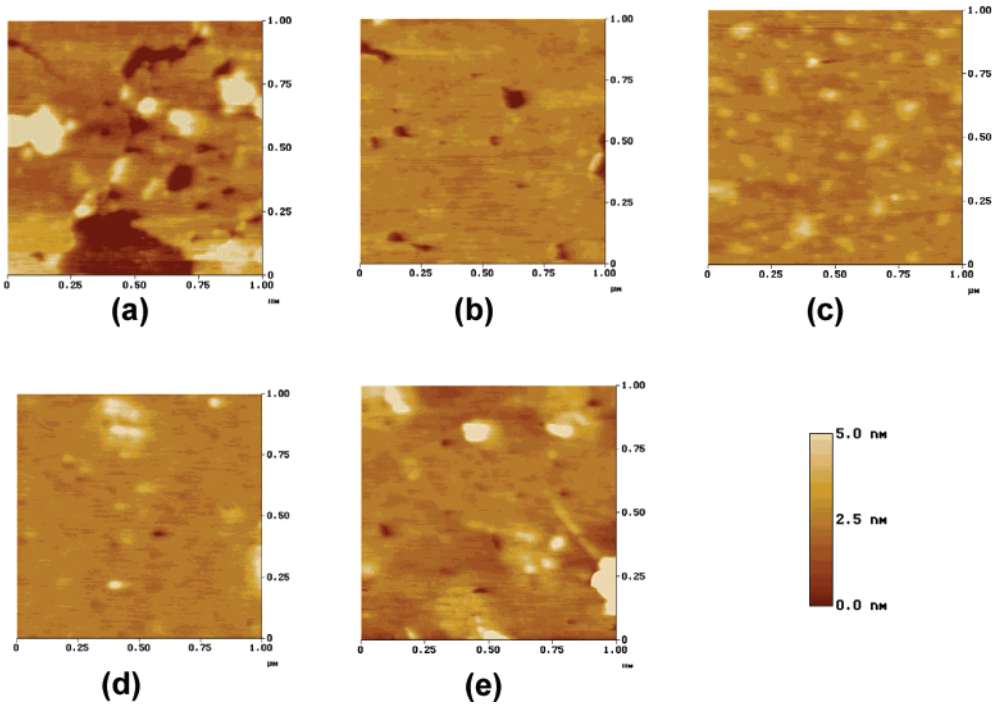

Figure 10. Atomic force microscopy images of the layers (only one horizontal lifting) of **1**/**TPPS$_4$** deposited onto hydrophobized silicon substrates at deposition pressure of 2 (a), 5 (b), 10 (c), 20 (d), and 25 (e) mN/m, respectively.

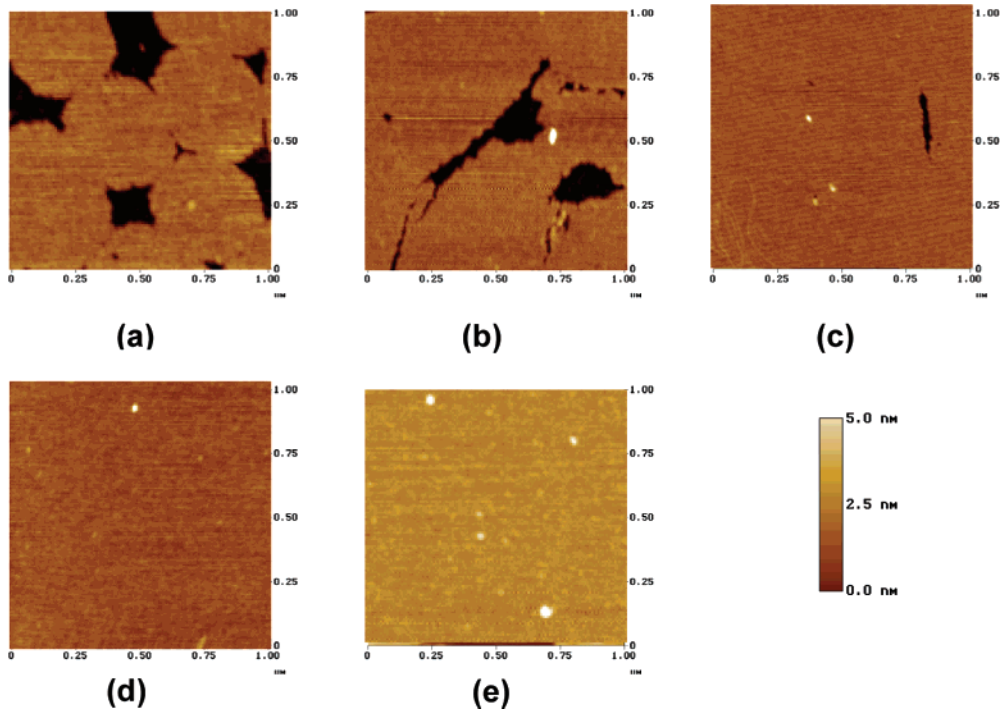

Figure 11. Atomic force microscopy images of the layers (only one horizontal lifting) of **2**/**TPPS$_4$** deposited onto hydrophobized silicon substrates at deposition pressure of 2 (a), 5 (b), 10 (c), 20 (d), and 25 (e) mN/m, respectively.

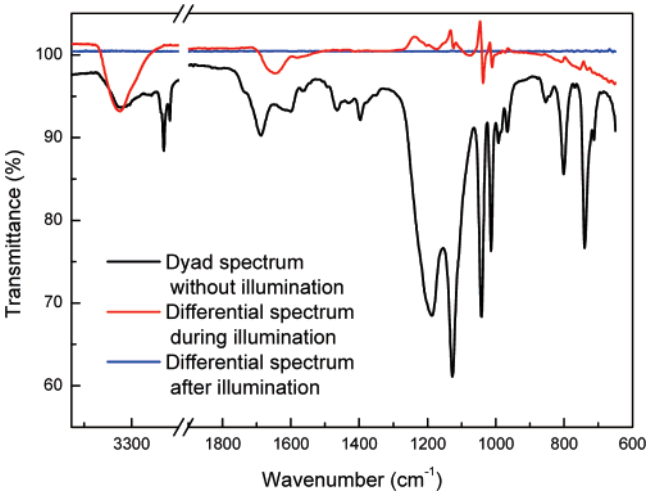

Figure 12. Differential spectra obtained before and after white light soaking (1500 W) on a LS film of the system **2**/**TPPS$_4$** deposited at 20 mN/m.

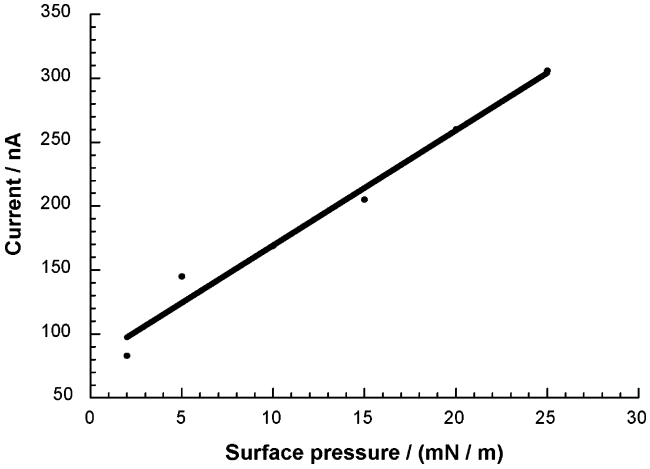

Figure 13. Surface pressure dependence of photocurrent for **ITO**/**2**/**TPPS$_4$**, under deoxygenated conditions (i.e., an aqueous solution containing 0.1 M Na_3PO_4 as supporting electrolyte and 1 mM ascorbic acid—no bias voltage is applied). Photocurrents were recorded upon monochromatic light illumination.

are hundreds of nanometer large and 5 nm high (Figure 11b). The measured rms is ca. 0.9 nm. The above-described defectivity decreases at deposition pressures of 10 mN/m (Figure 11c) and disappears at 20 and 25 mN/m (Figure 11d, e). The measured rms is in these last two cases ca. 0.3 and 0.4 nm, respectively. It is worth pointing out that the aforementioned AFM data are in good agreement with the BAM analysis, which showed **1**/**TPPS$_4$** aggregates densely and uniformly at deposition pressures lower than **2**/**TPPS$_4$**.

The first insight into possible electron transfer interactions in **2**/**TPPS$_4$**, LS film transferred at 20 mN/m by three LS runs, came from FT−IR attenuated total reflectance (ATR) spectrophotometry. A differential spectrum, that is, the difference between the film in the dark and that illuminated with white light at 1500 W, is depicted in Figure 12.[38,39]

In fact, in our case, signals at 1012 cm^{-1} and 1034 cm^{-1} correspond to the S−C group, while the signal at 1122 cm^{-1} is assigned to $-SO_2-O-$[40] and suggests that the sulfonate moieties are, indeed, involved in an electron transfer. The failure to detect any fullerene related features is due to the low reorganization energy of fullerenes in electron-transfer reactions.

Next, we investigated the accordingly modified ITO electrodes in photocurrent experiments, that is, measuring the response of light illumination (i.e., monochromatic or white light

(38) Iwaki, M.; Cotton, N. P. J.; Quirk, P. G.; Rich, P. R.; Jackson, J. B. *J. Am. Chem. Soc.* **2006**, *128*, 2621.
(39) Mäntele, W. *Biophysical Techniques in Photosynthesis*; Amesz, J., Hoff, A. J., Eds.; Kluwer Academic Publishers: Dordrecht, 1996; pp 137−160.
(40) Silverstein, R. M.; Webster, F. X.; Kiemle, D.; Kiemle, D. J. *Spectrometric Identification of Organic Compounds*, 10th ed.; John Wiley & Sons Inc.: New York, 2005.

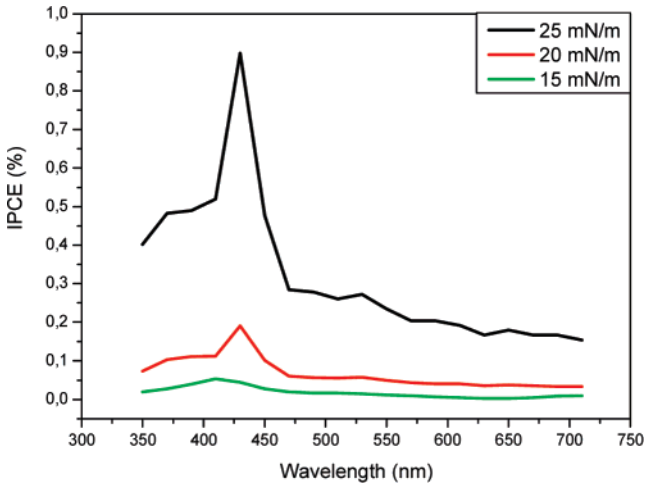

Figure 14. Photoaction spectrum of a modified ITO electrode bearing a single **2**/**TPPS$_4$** coverage at 15, 20, 25 mN/m, under deoxygenated conditions (i.e., an aqueous solution containing 0.1 M Na_3PO_4 as supporting electrolyte and 1 mM ascorbic acid—no bias voltage is applied). Photocurrents were recorded upon monochromatic light illumination.

illumination) on the generation of electrical energy. We like to emphasize that the following section deals exclusively with **ITO**/**2**/**TPPS$_4$** systems, in which the layers were produced at the water−air interface and transferred onto the ITO electrodes with only one LS run at a variety of surface pressures (i.e., 2 mN/m, 5 mN/m, 10 mN/m, 15 mN/m, 20 mN/m, and 25 mN/m); see Figure 13.

Immediately after the preparation, the photoaction spectra of the modified ITO electrodes were recorded under the following experimental conditions: 0.1 M Na_3PO_4, 1 mM ascorbic acid after nitrogen bubbling. This leads to photoaction spectra, for which a few representations of **ITO**/**2**/**TPPS$_4$** electrodes are reported in Figure 14.

Most importantly, an excellent match is noted with the absorption spectrum of **2**/**TPPS$_4$** at the air−water interface. The Soret bands (i.e., 425 nm) and also the Q-bands (i.e., 500−625 nm) of **TPPS$_4$** are noticeable. The features of **2**, on the other hand, are masked by the ITO absorption at wavelengths < 350 nm. With the photoaction spectrum in hand, we were able to confirm the origin of the photocurrents, namely, that the chromophoric activities of **TPPS$_4$** are mainly responsible for our observation.

Deposition of **2**/**TPPS$_4$** onto the ITO electrode places the primary electron acceptor, **2**, adjacent to the ITO electrode, while

Table 1. Active Photon to Current Efficiencies of **ITO/1/TPPS$_4$** and **ITO/2/TPPS$_4$** Electrodes

surface pressure	IPCE **ITO/1/TPPS$_4$**	IPCE **ITO/2/TPPS$_4$**	IPCE **ITO/1/TPP(PO$_3$H$_2$)$_4$**[a]
blank	------ (14 nA)	------ (10 nA)	------ (12 nA)
5 mN/m	0.085% (33 nA)	0.091% (35 nA)	0.038% (15 nA)
10 mN/m	0.1% (39 nA)	0.12% (46 nA)	0.043% (17 nA)
15 mN/m	0.13% (50.5 nA)	0.16% (62 nA)	0.048% (19 nA)
20 mN/m	0.18% (70 nA)	0.19% (73 nA)	0.060% (23 nA)
25 mN/m	0.21% (82 nA)	0.29% (112 nA)	0.064% (25 nA)

[a] Previous IPCEs obtained with a tetraphosphonate porphyrin are also reported for comparison.[32]

the electron donor, **TPPS$_4$**, sits in a remote position relative to the ITO electrode. Thus, within the context of photocurrent generation the following charge-transfer scenario develops: initial charge separation within the **2**/**TPPS$_4$** is followed by electron injection into the ITO electrode. Applying a positive bias at the ITO electrode surface is expected to facilitate the electron injection from the one-electron reduced electron acceptor (i.e., $C_{60}^{\bullet -}$). In fact, changing the bias from −500 mV to +500 mV vs Ag/AgCl (0.1 M KCl) (0.1 M Na_3PO_4, with ascorbic acid) leads to a tenfold increase of the photocurrent; see Figure 15.

Interestingly, the photocurrents increased notably with increasing surface pressure (see Figures 13 and 14) which corresponds to a closer packing of the dyad molecules. This observation can be rationalized on the grounds of higher absorption cross sections at higher surface pressures. Moreover, the higher IPCE efficiencies observed in the current **ITO**/**2**/**TPPS$_4$** relative to **ITO**/**1**/**TPPS$_4$** are attributed to a tighter/stronger donor−acceptor complex formation. Evidently, the larger number of charges residing at the functional groups of **2** favors a more efficient electron transfer. After transforming the photocurrents into IPCE percentage we obtained the magnitudes presented in the following Table.

To probe the stability of the photocurrents, an **ITO**/**2**/**TPPS$_4$** electrode was illuminated over several time intervals. Only the $CuSO_4$ filter was employed to cutoff the wavelength region that would correspond to the illumination of the ITO electrode itself. Importantly, the response to ON/OFF cycling (i.e., turning the light source on and off) is prompt and reproducible; three cycles are shown in Figure 16. Over the monitored time window of 60 s a moderate increase in current of less than 5% was noted, which is due to diffusion of ascorbic acid.

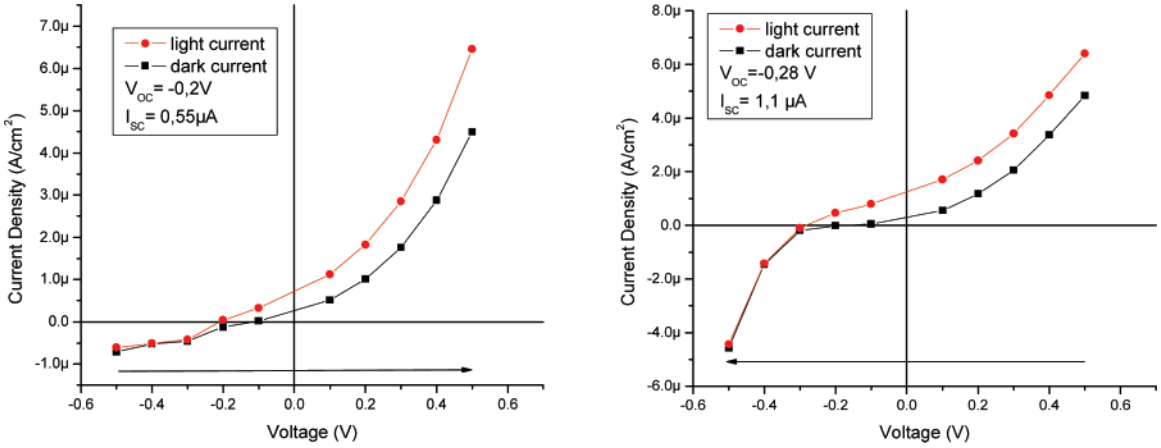

Figure 15. Current voltage characterization (in a forward and reverse mode, respectively) of the **2**/**TPPS$_4$** LS film deposited at 25 mN/m onto ITO support.

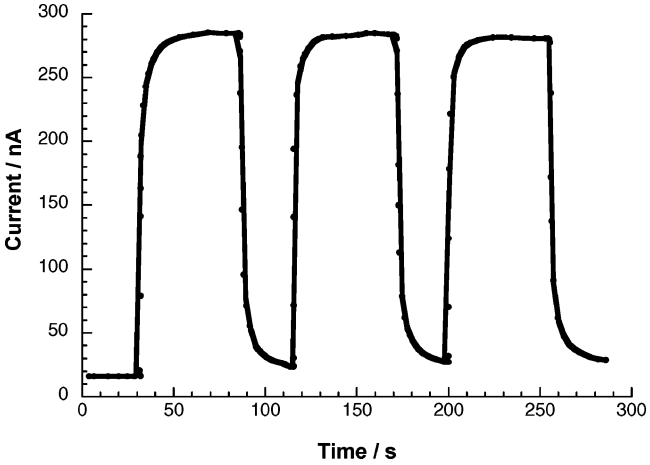

Figure 16. Photocurrent generation from ITO electrodes bearing a single **2**/**TPPS$_4$** LS deposition on ITO, under visible light irradiation/deoxygenated conditions (i.e., an aqueous solution containing 0.1 M Na_3PO_4 as supporting electrolyte and 1 mM ascorbic acid—no bias voltage is applied). Photocurrents were recorded upon visible light illumination.

Conclusions

We have constructed mixed composite thin films consisting of cationic fulleropyrrolidine derivatives **1** and **2** and a commercial anionic porphyrin derivative, **TPPS$_4$**, dissolved in the subphase. We have fabricated high-quality, robust, and photoactive films by making use of the horizontal lifting method and electrostatic interactions. To the best of our knowledge we have for the first time organized such moieties through this unique and powerful procedure. Moreover, such a combination of donor and acceptor moieties held in close proximity by electrostatic interactions leads to photocurrent generations that exhibited a meaningful efficiency increase with increasing transfer pressures. Even a noteworthy dependence on the cation-to-anion charge ratio has been evidenced, since magnification of IPCE values has been monitored even upon enhancement of the coulomb forces between the fullerene derivatives and **TPPS$_4$**. Finally the nonconventional differential spectroscopy in the FT−IR attenuated total reflectance (ATR) mode has revealed that probably the sulfonate functionalization is involved in the electron transfer.

In conclusion, all these experimental observations suggest the utilization of the described method of deposition as a new effective tool for the fabrication of functioning devices that contain fullerene and macrocyclic derivatives as active species for photocurrent generation. Our research is currently proceeding by inversion of the specified approach using new, charged, and water soluble fullerene derivatives and porphyrinic charged moieties at the air−water interface. Also change of the cation-to-anion ratio, together with variation of previously specified transfer conditions, will be taken into account in order to control how such parameters reflect on molecular organization and vary the film response to light illumination.

Acknowledgment. The authors wish to thank Luigi Dimo (University of Lecce) for his technical support during Langmuir experiments. This work was carried out with partial support from the University of Trieste and MiUR (PRIN 2006, prot. 2006034372 and prot. 2006031909_002), EU (RTN networks "WONDERFULL" and "CASSIUSCLAYS"), the Department of Energy Basic Science program (document NDRL-4711 from the Notre Dame Radiation Laboratory), and from the University of Lecce (Ricerca di Base).

Supporting Information Available: Experimental details (PDF). This material is available via the Internet at http://pubs.acs.org.

JA0655789